PNAS RESEARCH ARTICLE | MEDICAL SCIENCES

# Expanded profiling of WD repeat domain 5 inhibitors reveals actionable strategies for the treatment of hematologic malignancies

Christian T. Meyer[a,b,1], Brianna N. Smith[c,1], Jing Wang[d,e], Kevin B. Teuscher[f], Brian C. Grieb[g], Gregory C. Howard[h], Alexander J. Silver[g], Shelly L. Lorey[h], Gordon M. Stott[i], William J. Moore[j], Taekyu Lee[f], Michael R. Savona[g], April M. Weissmiller[k], Qi Liu[d,e], Vito Quaranta[b,f], Stephen W. Fesik[f,l,m], and William P. Tansey[f,h,2]

Affiliations are included on p. 10.

Edited by Alexander Varshavsky, California Institute of Technology, Pasadena, CA; received May 3, 2024; accepted July 25, 2024

**WD40 Repeat Domain 5 (WDR5) is a highly conserved nuclear protein that recruits MYC oncoprotein transcription factors to chromatin to stimulate ribosomal protein gene expression. WDR5 is tethered to chromatin via an arginine-binding cavity known as the "WIN" site. Multiple pharmacological inhibitors of the WDR5-interaction site of WDR5 (WINi) have been described, including those with picomolar affinity and oral bioavailability in mice. Thus far, however, WINi have only been shown to be effective against a number of rare cancer types retaining wild-type p53. To explore the full potential of WINi for cancer therapy, we systematically profiled WINi across a panel of cancer cells, alone and in combination with other agents. We report that WINi are unexpectedly active against cells derived from both solid and blood-borne cancers, including those with mutant p53. Among hematologic malignancies, we find that WINi are effective as a single agent against leukemia and diffuse large B cell lymphoma xenograft models, and can be combined with the approved drug venetoclax to suppress disseminated acute myeloid leukemia in vivo. These studies reveal actionable strategies for the application of WINi to treat blood-borne cancers and forecast expanded utility of WINi against other cancer types.**

WDR5 | cancer therapy | ribosomes | venetoclax | lymphoma

## Significance

WD40 Repeat Domain 5 (WDR5) is a cofactor for myelocytomatosis (MYC) oncoproteins and a promising target for cancer therapy. Drug-like inhibitors of the WDR5-interaction (WIN) site of WDR5 have been described, but have only been shown to be active against a handful of rare cancer types. By expanded profiling of WINi in diverse cancer contexts, we find these agents are active in a variety of malignant settings, with particular efficacy against leukemia and diffuse large B cell lymphoma. We also show that WINi synergize with the approved drug venetoclax to suppress leukemia progression in mice. Our studies reveal that indications for WINi as anticancer agents are broader than currently thought, and provide a roadmap to support their clinical implementation.

WD Repeat Domain 5 (WDR5) is a highly conserved nuclear protein that has gained prominence as a target for anticancer drug discovery (1). Its best-known role is to scaffold the MLL/SET (mixed lineage leukemia/Su(var)3-9, E(z) and Trithorax) histone methyltransferase (HMT) complexes that methylate histone H3 lysine four, but WDR5 also scaffolds other epigenetic writer complexes and recruits MYC oncoproteins to chromatin to stimulate ribosomal protein gene (RPG) transcription (2). Strategies to pharmacologically inhibit WDR5 are based on targeting one of two sites—the WDR5-binding motif site and the WDR5-interaction (WIN) site—that mediate interactions with partner proteins (2). Most drug discovery campaigns target the WIN site (1), an arginine-binding cavity that tethers WDR5 to chromatin (3) and engages arginine-containing WIN motifs found in proteins such as the MLL/SET HMT enzymes (4). Multiple small-molecule WIN site inhibitors (WINi) have been discovered (1), including those that are orally bioavailable, efficacious, and safe in rodents (5), forecasting that WINi will be ready for clinical vetting in the near future.

Despite progress in drug discovery, the cancer types in which WINi have documented efficacy are small and confined to rare cancers such as neuroblastoma (6), rhabdoid tumors (7), and MLL-rearranged (MLLr) acute myeloid leukemia (AML) (3, 8). Two factors make it difficult to know whether these cancer types represent the totality of those sensitive to WINi, or if there are other malignant settings in which these agents may be of benefit. First is the finding that WINi disrupt only a specific subset of WDR5 activities (9) and are thus selective loss of function agents. This selectivity may underlie their safety in vivo (5)—permitting a "common essential" protein such as WDR5 (10) to be inhibited without broad toxicity—but it also means that genome-wide resources (10), or individual studies of WDR5 knockout/knockdown, cannot be used to predict which cancer cell types will be sensitive to WIN site blockade (1). The second major factor is their unique mechanism of action, which sets WINi apart from other approved and experimental anticancer drugs (1). Our studies of WINi showed that they act in AML cells by evicting WDR5 from chromatin at MYC-driven RPGs, suppressing RPG transcription, and inducing p53-mediated apoptosis via a nucleolar stress response (3, 11, 12). Although strategies

This article is a PNAS Direct Submission.



[1]C.T.M. and B.N.S. contributed equally to this work.

[2]To whom correspondence may be addressed. Email: william.p.tansey@vanderbilt.edu.

This article contains supporting information online at https://www.pnas.org/lookup/suppl/doi:10.1073/pnas.2408889121/-/DCSupplemental.

Published August 21, 2024.

have been proposed to exploit heightened ribosome biogenesis for cancer therapy (13), none—apart from WINi—act via direct RPG suppression and p53 induction. As a result, there is little precedent with which to guide deployment of these agents, as well as concerns that their utility will be limited to those cancers with intact p53 signaling.

We reasoned that the most effective way to expose the single agent utility of WINi is to profile them against a diverse panel of cancer cell lines. We also reasoned that any application of WINi for cancer therapy will likely be made as part of a drug combination strategy and that identifying synergies—particularly with a US Food and Drug Administration (FDA)-approved anticancer drug—would accelerate their clinical implementation. Here, we screened WINi across a panel of 300 cancer cell lines derived from 20 different cancer types. We show that WINi are active against select solid and hematologic tumor cell lines in vitro, with the largest sensitive groups derived from leukemias and diffuse large B cell lymphomas (DLBCL). We also report that sensitivity of hematologic cancer cells to WINi correlates with RPG expression, that the requirement for wild-type (WT) p53 for response to WINi is not absolute, and that WINi are synergistic with the FDA-approved agent venetoclax against AML in vitro and in vivo. Together, these findings reveal that the indications for WINi as a targeted anticancer therapy are broader than currently thought, and provide a roadmap to support their clinical implementation.

## Results

**Screening Chemically Diverse WINi against the OncoSignature Cancer Cell Panel.** We screened WINi against 301 cancer lines in Horizon OncoSignature 2D Cell Panel, representing ~20 different cancer types (Dataset S1), a majority of which are derived from solid tumors (Fig. 1*A*). For added rigor, we profiled three distinct WINi: **C38b**, **C3b**, and **C40**. These WINi each carry a bicyclic dihydroisoquinolinone core (14) that locks the inhibitor into a favorable conformation for engaging WDR5, but differ in pharmacophores that engage the $S_2$ and $S_7$ subsites in the WIN site (*SI Appendix*, Fig. S1*A*). Compared to compound **C6**, which has been used in a majority of studies to date (3, 6, 7, 11), these WINi are significantly more potent. They bind WDR5 with an affinity at or below the limit of quantitation of a time-resolved fluorescence energy transfer (TR-FRET) assay ($K_i \leq 20$ pM) and display low nanomolar efficacy against benchmark MLLr lines MV4:11 and MOLM-13 in vitro (*SI Appendix*, Fig. S1*B*). By screening with three chemically diverse WINi, we could identify high-confidence sensitivities across different cell types.

Cells were treated for 5 d with a 14-point dilution series of each inhibitor in triplicate and compound activity expressed as area under the dose–response curve (AUC) or observed maximal efficacy (Emax), where 100% is a cytostatic response and 200% is complete cytotoxicity (Dataset S1). Both AUC and Emax were determined based on the fitted dose–response curve (four-parameter Hill equation). In total, the screen comprised 40,593 measurements. Over 90% of dose–response curves fit with an $R^2 > 0.6$, demonstrative of the quality of the screen (*SI Appendix*, Fig. S1*C*). Despite WDR5 being essential in the vast majority of cell lines screened—as evidenced by Chronos scores of around −1.0 (10, 15)—most cell lines profiled are relatively insensitive to all three agents (AUC < 20; Fig. 1*B*). Indeed, there is no correlation between the essentiality of WDR5 and the response to WINi (*SI Appendix*, Fig. S1*D*), reinforcing the notion that WINi impact only part of WDR5 function, and that WDR5 knockout studies cannot and should not be used to predict cancer cell response to WIN site blockade (1).

All three WINi display similar AUC response profiles (Fig. 1*B*), indicative of a shared mechanism of action. It is clear, however, that **C3b** and **C38b** are more correlated to each other than to **C40** (the least potent of the three), as judged by both AUC (Fig. 1*C*) and Emax (Fig. 1*D*). Stratifying by median AUC (Fig. 1*E* and *SI Appendix*, Fig. S1*E*), we see that—as expected—MLLr and rhabdoid lines are sensitive to all three agents (Dataset S1), supporting the validity of the screen. Notably, we also observe robust activity in a number of lines derived from solid malignancies—most prominently ovarian and breast cancer. The unexpected finding that lines from these cancer types are sensitive to WINi indicates that these agents may be efficacious against a subset of solid malignancies with a significant clinical burden.

In general, however, leukemia and lymphoma lines stand out as most sensitive to WINi: Among the 90th percentile of responders, half are derived from hematologic malignancies (Fig. 1*F*). Leukemia and lymphoma lines also stand out as sensitive based on Emax (*SI Appendix*, Fig. S1*F*). Curation of the top 25 sensitive lines (Fig. 1*G*) reveals that one third are derived from DLBCL, and that within this tier most lines exhibit a cytotoxic response, as evidenced by Emax values > 100. Although some DLBCL lines are insensitive to WINi, the strong representation of DLBCL lines—including those derived from difficult-to-treat double-hit lymphomas [e.g., SU-DHL-6, DOHH-2, OCI-LY-10; (16)]—in this sensitive cohort reveals this context is one in which WINi should be prioritized for clinical utility.

**Response to WINi Correlates with Protein Synthesis Gene Expression But Is Not Dependent on Functional p53.** Prior studies documented the importance of WT p53 for a robust response to WINi. And yet half the lines in the sensitive tier harbor *TP53* mutations, most of which are predicted to be pathogenic (Fig. 1*G*)—demonstrating that WT p53 is not, as currently thought, a requisite to the inhibitory effects of WINi in cancer cells. To better explore the relationship between p53 and response to WINi, we queried *TP53* status across the panel. Because mutations in *RPL22* are associated with inactivation of p53 via alternative splicing of MDM4 messenger RNA (mRNA) (12, 17), we included *RPL22* mutation status in our analysis. Across all lines, the presence of WT p53/RPL22 is associated with a higher response AUC (Fig. 2*A*). Breaking down by cancer type, however, reveals that trends between p53/RPL22 status and response to WINi are cancer type selective, and only reach significance for all three agents in leukemia lines (Fig. 2 *B*–*D*). This analysis implies that the general vulnerability of leukemia cells to WINi is dependent on their ability to mount a p53 response, as we have reported in MLLr cells (3). Why leukemia cells show this correlation is unclear, although as leukemias such as AML (18) and acute lymphoblastic leukemia (ALL) (19) are typically WT for p53 at diagnosis, this finding suggests that WINi could be part of a first-line treatment in these cancers.

Next, we probed for association of hematologic cancer cell line sensitivity to WINi with mRNA expression levels reported in the Cancer Cell Line Encyclopedia (CCLE) (17, 20). To compute significance, correlations were compared to a scrambled gene set (Fig. 2*E*). In total, we identified 18 positive and ~800 negative significant gene expression correlations across all three WINi (Dataset S1). Remarkably, genes correlated in each direction are connected to protein synthesis. Of the 18 positively correlated genes, 12 encode ribosomal proteins (Fig. 2 *F* and *G*). Among the negatively correlated genes, we observe strong enrichment in Gene Ontology (GO) categories relating to RNA processing, ribosome biogenesis, and the nucleolus (Fig. 2*H*) including genes encoding subunits of RNA polymerase I

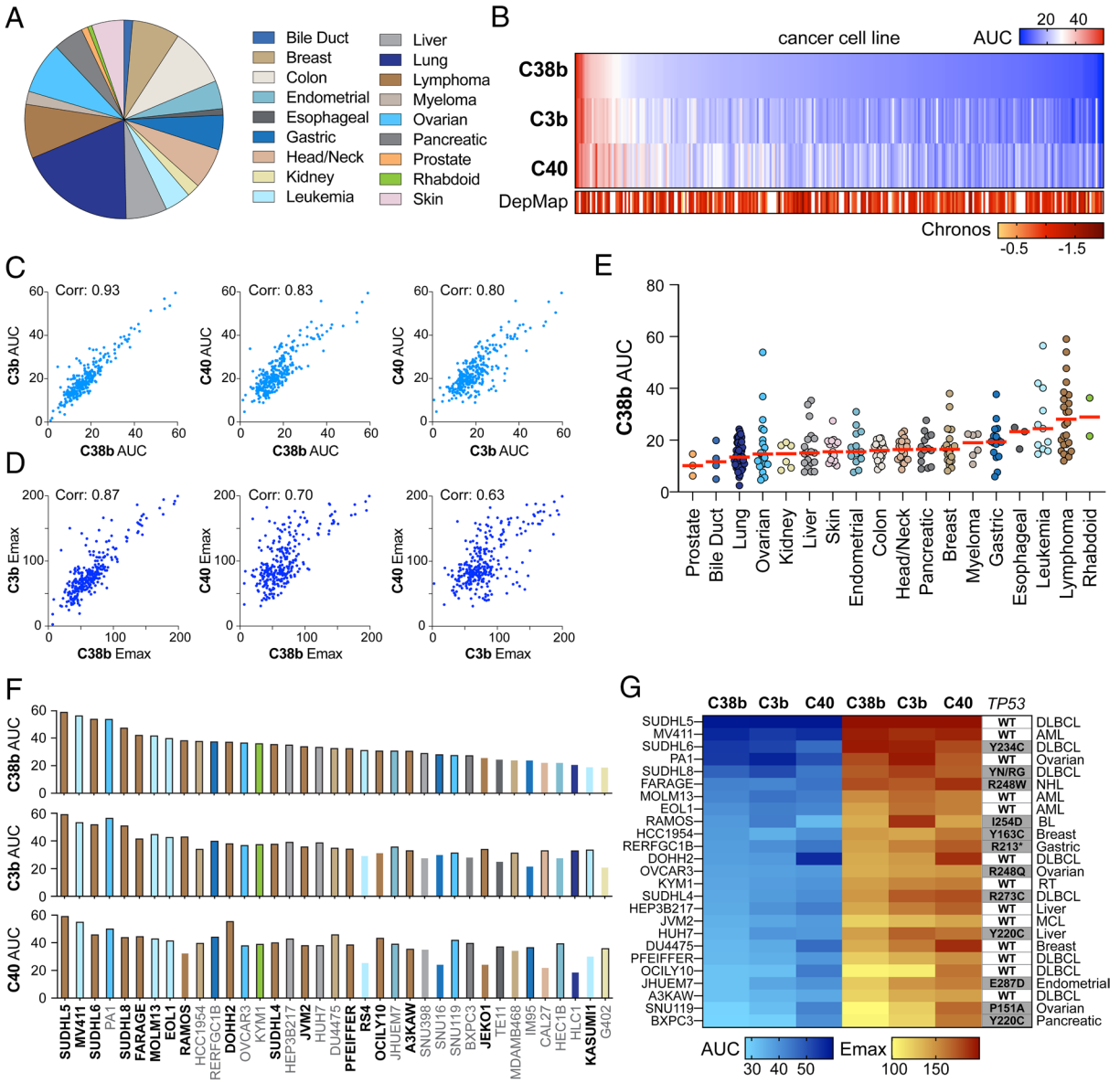


**Fig. 1.** Screening chemically diverse WINi against the OncoSignature Cancer Cell Panel. (*A*) Cell lines in the OncoSignature Panel by cancer type. (*B*) Heatmap, displaying area under the dose-response curve (AUC) for cell lines treated with a dilution series of the indicated WINi for five days ($n$ = 3 to 6). Chronos scores for the 222 cell lines shared between the Oncosignature Panel and the DepMap resource are shown beneath. Cell lines not represented in DepMap are in white. A Chronos score of −1.0 corresponds to the median of all common essential genes. (*C*) Correlation plots of AUC for all pairwise combinations of WINi. Correlation value for each is the Pearson-r. (*D*) Correlation plots of Emax for all pairwise combinations of WINi. Correlation value for each is the Pearson-r. (*E*) Swarmplot, displaying calculated AUC for **C38b**, clustered by cancer type. The red line indicates median AUC for each cancer type. Color-coding as in *A*. (*F*) AUC for indicated cell lines in the 90th percentile for each WINi, ranked by **C38b**. Outlined bars are in the 90th percentile for the indicated agent; open bars are in the 90th percentile for one or more of the other agents only. Heme cancer line names are bolded. Color-coding as in *A*. (*G*) Heatmap, displaying AUC/Emax for each agent in the top 25 most-responsive cell lines. *TP53* status is from the CCLE and shows either WT or the affected p53 protein residue. SUDHL8 cells carry two p53 mutations (R249G/Y234N; designated "YN/RG"). "R213*" indicates a frameshift in p53 at residue 213. NHL—non-Hodgkin lymphoma, BL—Burkitt lymphoma, RT—rhabdoid tumor, MCL—mantle cell lymphoma.

(POLR1A/B) and factors required for rRNA maturation (e.g., PES1) (Dataset S1). We also observe modest but significant enrichment in genes encoding switch/sucrose nonfermenting (SWI/SNF) components, and in gene categories identical to those suppressed by WINi (3, 6, 7), including MYC targets and the G2M checkpoint (Dataset S1). The representation of translation-linked genes in both the positively and negatively correlated gene sets provides further support for the idea that the action of WINi, in the context of hematologic malignancies, is tied to their ability to modulate MYC-driven RPG expression and thus cancer cell protein synthesis capacity.

**Hematologic Cancer Lines Are Sensitive to WINi In Vivo.** Our previous in vivo testing of WINi was confined to the MLLr leukemia line MV4:11 (5). Results from the screen, however, prompted us to examine the sensitivity of additional hematologic cancer lines in subcutaneous mouse xenograft assays. For this purpose, we selected our recently developed, orally bioavailable, WINi **C10**, which carries an imidazole $P_2$ warhead and is similar in affinity and in vitro potency to the three WINi profiled in the cell panel screen (5). We dosed **C10** by oral gavage at 100 mg/kg either daily (QD) or twice daily (BID), once engrafted tumors had reached ~150 to 300 $mm^3$.

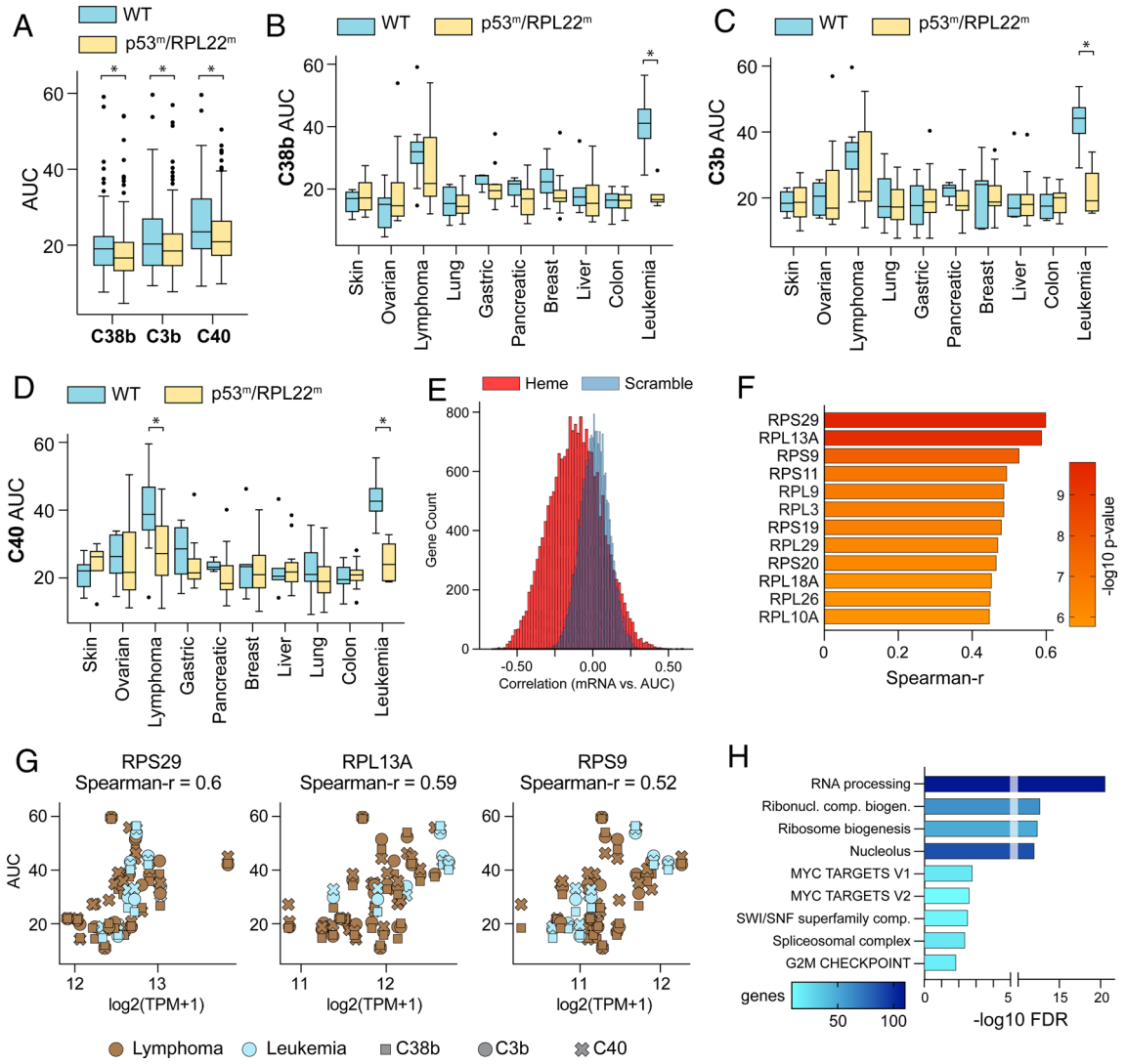


**Fig. 2.** WINi response is correlated with protein synthesis gene expression but does not depend on WT p53 status. (*A*) Boxplot, displaying AUC for each agent for all cell lines broken down by whether they carry WT or mutant p53/RPL22. Boxes cover the 25th and 75th percentiles; the middle line marks the median. Whiskers represent three SD from the mean and values exceeding this deviation are marked as outliers (Mann–Whitney *U* rank sum test, $*P \leq 0.05$). (*B*) As in *A* but for **C38b** and broken down by cancer type. Each subtype is split into those carrying mutations in either *TP53* ($p53^m$) or *RPL22* ($RPL22^m$) (gold) versus cell lines without mutations in either gene (blue) according to the CCLE database. Boxes cover the 25th to 75th percentiles of the data; the middle line is the median. Whiskers are three-SD from the mean and points depict outliers. Statistical significance (*) was determined using a one-sided Mann–Whitney *U* rank sum test, *P*-val < 0.05. Boxplot analysis is also shown for **C3b** (*C*) and **C40** (*D*). (*E*) To determine the statistical significance of gene expression correlation to drug activity (AUC), the distribution of correlations was compared to the distribution arising from a randomly scrambled gene set. The z-score is defined as the value minus the mean of the scramble control divided by the SD of the scramble control. (*F*) Graph shows Spearman-r correlation values (*x*-axis) and *P*-value (−log10; color) for the 12 RPGs for which expression is positively correlated to AUC across all three WINi. (*G*) WINi activity (AUC) correlated to mRNA expression in the CCLE. Correlation calculated using Spearman-r. (*H*) Output of gene enrichment analysis for genes negatively correlated to AUC across all WINi. Color represents recovered gene count; the *x*-axis represents −log10 of the false discovery rate (FDR).

Four WINi-sensitive cancer lines were profiled in vivo: MV4:11, EOL-1 (eosinophilic leukemia), Jeko-1 (mantle cell lymphoma), and SU-DHL-5 (DLBCL; germinal center B cell subtype). MV4:11 cell tumors responded in vivo as expected (5), displaying a significant reduction in volume as early as 4 d after treatment initiation (Fig. 3*A*) and completing the treatment course at roughly one third the volume of the vehicle control group. Early on, MV4:11 tumor growth inhibition (TGI) reached ~100% (*SI Appendix*, Fig. S2*A*), but this was followed by a period in which TGI was between 60 to 70%, depending on dosing regimen. As observed previously (5), **C10** was well tolerated during the treatment period, with mice showing no signs of clinical abnormalities or significant weight loss (Fig. 3*A*). EOL-1 tumors exhibited similar response characteristics (Fig. 3*B*), although the level of TGI was less than that of other heme line xenografts, with TGI peaking at 50% for BID dosing (*SI Appendix*, Fig. S2*B*).

Crucially, the two remaining lines show a more robust response to **C10** than MV4:11 cells. Indeed, the growth of both Jeko-1 (Fig. 3*C*) and SU-DHL-5 (Fig. 3*D*) xenografts are rapidly and durably suppressed by **C10**, with TGI remaining at ~80% for Jeko-1 (*SI Appendix*, Fig. S2*C*), and almost 100% for SU-DHL-5 (*SI Appendix*, Fig. S2*D*). Mice in the BID-treated SU-DHL-5 tumors lost on average 3% of body weight across the treatment course (Fig. 3*D*) but showed no other obvious abnormalities. Interestingly, although SU-DHL-5 cells express WT p53 (Fig. 1*G*), Jeko-1 cells carry pathogenic TP53 mutations (21) and are resistant to MDM2 inhibitors (22), again supporting the idea that, depending on the context, p53 is not essential for tumor suppression by WINi. Taken together, these studies bolster the concept that WINi have broader single agent clinical utility than previously conceived, especially in the context of difficult-to-treat lymphomas and cancers bereft of WT p53.

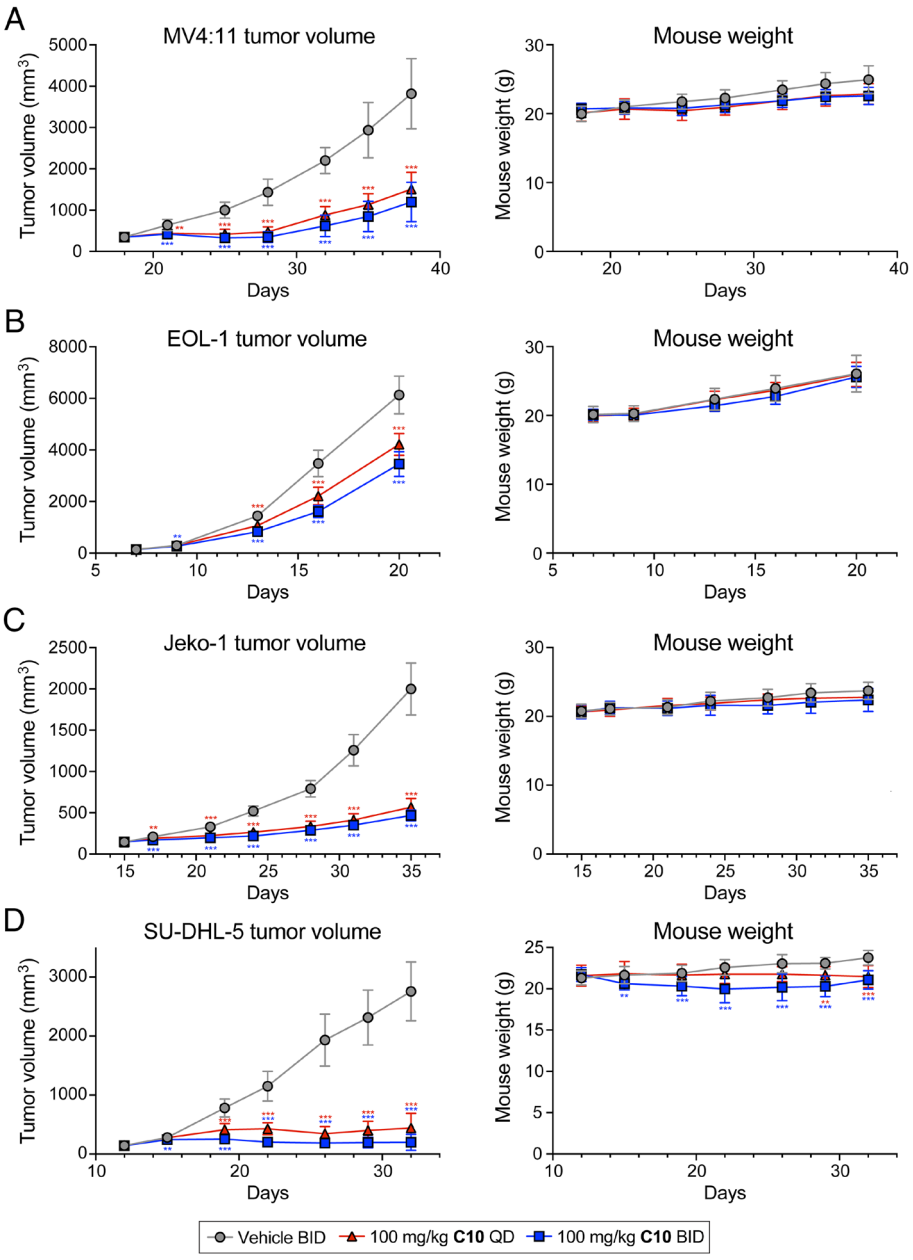


**Fig. 3.** Heme cancer lines are sensitive to WINi in vivo. (*A*, *Left*) Mean tumor volumes of MV4:11 xenografts in BALB/c nude mice after QD or BID dosing of **C10** at 100 mg/kg or vehicle control. Treatment started 18 d after tumor inoculation. (*Right*) Mean mouse weight. Error bars are SEM; $n = 10$ mice per group. Statistical significance was assessed via *t* test. $^{**}P < 0.005$; $^{***}P < 0.001$. (*B*) As in *A* except for EOL-1 xenografts. Treatment started 7 d after inoculation. (*C*) As in *A* except for Jeko-1 xenografts. Treatment started 15 d after inoculation. (*D*) As in *A* except for SU-DHL-5 xenografts. Treatment started 12 d after inoculation.

**WINi Are Synergistic with Multiple Agents in Leukemia Cells.** In line with current practice (23), future application of WINi for cancer therapy will likely be made as part of a drug combination strategy. To identify combinations that may be effective in hematologic malignancies, we next screened **C10** in combination with 10 agents—referred to here as "adjuvants"—in five leukemia and six lymphoma cell lines (Fig. 4*A*). Adjuvants were selected from standards of care or experimental agents for which there are expectations for synergy (Dataset S2). Cells were treated for 5 d with combinations in an 8 × 8 dose matrix in triplicate. In total, the screen comprised 21,120 measurements. Synergy was calculated via the MuSyC algorithm (24, 25), which separates synergistic efficacy (increases in therapeutic effects) from synergistic potency (decreases in therapeutic dosing). Output of the MuSyC analysis is in Dataset S2.

Synergy screening data are well fit by the two dimensional (2D) Hill equation employed by MuSyC, with 99% of combinations tested having an $R^2 > 0.6$ (*SI Appendix*, Fig. S3*A*). The single agent activity of **C10** in this panel (Fig. 4*B*) ranges from moderately cytostatic in p53-mutant HEL 92.1.7 leukemia cells (*SI Appendix*, Fig. S3*B*) to completely cytotoxic in lines such as MV4:11, MOLM-13, and SU-DHL-5, mirroring the behavior of WINi observed in the first screen. To identify combinations that cause significant cell killing, we selected those that achieve a median of >175% growth inhibition at the highest doses tested (Fig. 4*C*; dotted line). Menin, DOT1L, and PRMT5 inhibitors were excluded based on this criterion. This step prevents identifying synergistic but weakly efficacious combinations by considering the magnitude of the combination effect prior to prioritizing by synergy. Because the remaining adjuvants are highly efficacious as

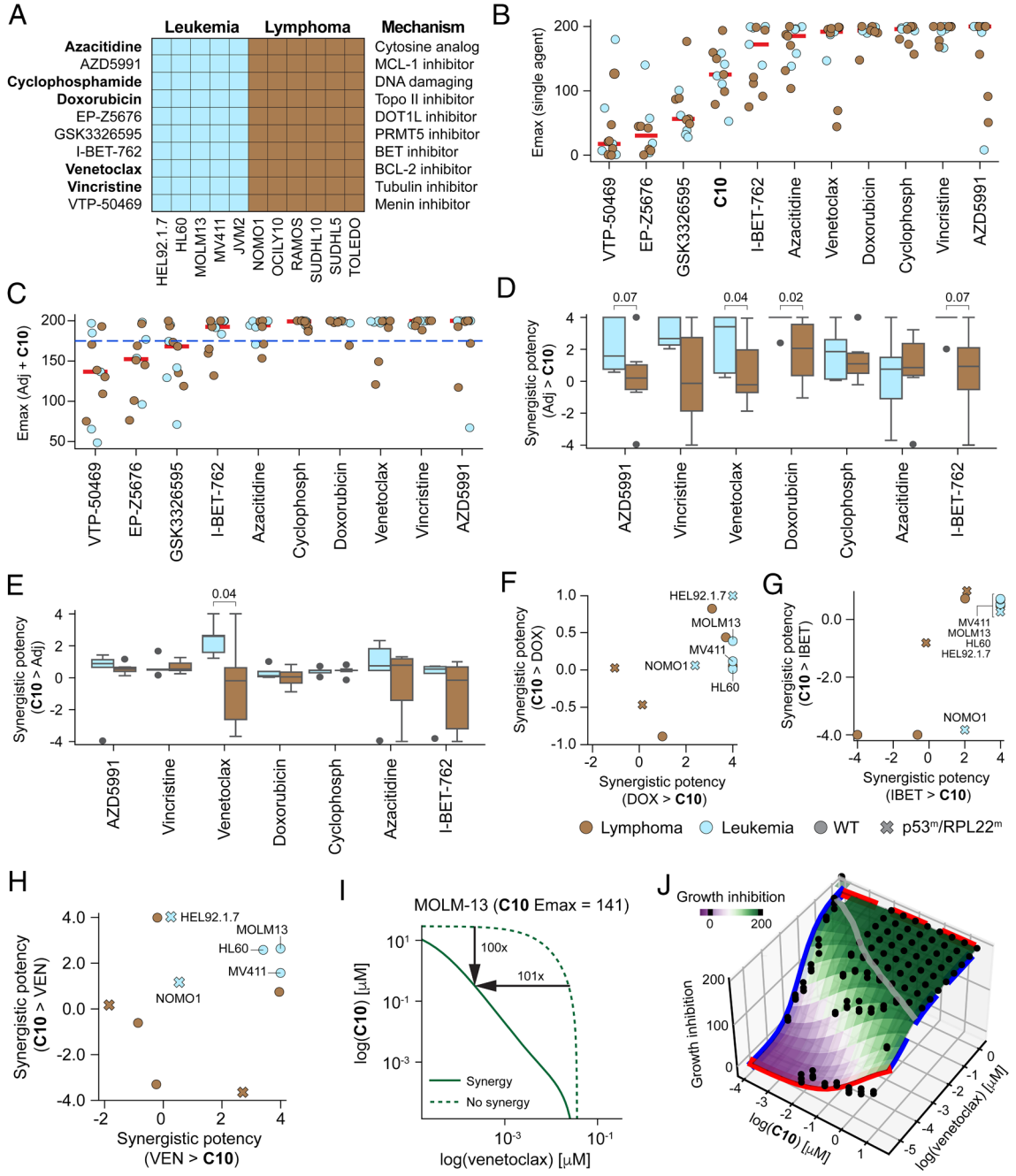


**Fig. 4.** WINi are synergistic with multiple agents in leukemia cells. (*A*) Synergy screen adjuvants and cell lines. Adjuvants in bold are FDA-approved. All combinations were tested in biological triplicate. (*B*) Maximal effect (Emax) of each agent alone. The red bar denotes median Emax. Cancer types color-coded as in *A*. (*C*) Maximal effects of **C10** in combination with each of the adjuvants (Adj) at the highest doses. The red bar denotes median Emax for each combination. The dotted line indicates the threshold (175% growth inhibition) for selecting efficacious combinations. (*D*) Boxplot of synergistic potency for each adjuvant by cancer type. Synergistic potency is equal to the log10 change in potency of **C10** in saturating concentrations of the adjuvant. *P*-values are calculated using a one-sided Mann–Whitney *U* rank sum test. Boxplot computed by quartiles. The bar marks the median. Outliers are included in statistical test. (*E*) As in *D* but showing the log10 change in the potency of each adjuvant in saturating concentrations of **C10**. (*F*) Synergistic potency scatterplot for doxorubicin (DOX). "**C10** > DOX" denotes the impact of **C10** on the potency of doxorubicin. "DOX > **C10**" denotes the impact of doxorubicin on the potency of **C10**. Symbols represent cancer type and p53/RPL22 status. Only leukemia lines are labeled. (*G*) As in *F* but for **C10** and I-BET-762 (IBET). (*H*) As in *F* but for **C10** and venetoclax (VEN). (*I*) MuSyC isobole analysis of the combination of **C10** and venetoclax in MOLM-13 cells. Dose combinations required to maintain the maximal effect of **C10** alone (Emax = 141) are traced by lines, with (solid) or without (dashed) synergy. The bidirectional synergistic potency enables lowering **C10** by 100-fold and venetoclax by 101-fold compared to the no synergy case. (*J*) MuSyC dose–response surface for the combination of **C10** and venetoclax in MOLM-13 cells. Colormap corresponds to percent growth inhibition according to the MuSyC equation fit to the experimental data (black dots). The gray line marks the contour of 190% inhibition. Black dots are the experimental data. Solid blue and red lines show the dose–response curves for venetoclax and **C10** alone, respectively.

single agents (Fig. 4*B*), we observed no strong synergy of efficacy across the panel (*SI Appendix*, Fig. S3*C*), and therefore focused our efforts on combinations that yield synergy of potency.

All adjuvants tested displayed some synergy of potency with **C10** in at least one cell line (Dataset S2). In general, when synergy is observed, it results from the adjuvant increasing the potency of **C10** (Fig. 4*D*), rather than vice versa (Fig. 4*E*). Synergy of potency is more pronounced in the leukemia lines, where we observe large and consistent synergies with venetoclax, doxorubicin, and I-BET-762 (Fig. 4*D*). The finding that three mechanistically

diverse agents can enhance the potency of WINi reveals that interference with multiple processes and pathways can sensitize cells to the cytotoxic effects of WIN site blockade. Both doxorubicin (Fig. 4*F*) and I-BET-762 (Fig. 4*G*) increase the potency of **C10** by ~10,000-fold (synergy score ~4) in four of the five leukemia lines, with the exception of NOMO-1, which carries a frameshift mutation in p53 (*SI Appendix*, Fig. S3*B*). The synergies in these instances could be explained by the fact that WINi (3), doxorubicin (26), and Bromodomain and Extra-Terminal motif (BET)-bromodomain inhibitors (27) all induce or augment induction of p53 as part of their mechanism of action.

Synergy of potency with the BCL-2 inhibitor venetoclax (28) in leukemia cells is also robust (Fig. 4 *D* and *E*), except here synergy is bidirectional and aligned with WT p53/RPL22 status (Fig. 4*H*). To compute the absolute dose reduction enabled by the combination of **C10** and venetoclax in these leukemia lines, we developed an analysis based on MuSyC isoboles, determining the doses of **C10** and venetoclax required to achieve the same effect possible with **C10** alone, with and without synergy. In MOLM-13 cells, the observed maximal efficacy of **C10** as a single agent is ~140, which occurs at the highest dose of 30 μM. In combination with venetoclax, the same effect is achieved with 100 times less **C10**, and at a dose of venetoclax that is 101 times lower than would be required in the absence of synergy (Fig. 4*I*). This high synergistic activity results in near-complete growth inhibition (>190%) of MOLM-13 cells at 300 nM **C10** and 2 nM venetoclax (Fig. 4*J*). Similar effects were observed in the other two sensitive leukemia lines, with comparable maximal effects achieved at 100 times less **C10** and more than 15 times less venetoclax (*SI Appendix*, Fig. S3 *D* and *E*). In contrast, p53-mutant NOMO-1 cells showed no synergy between the two agents. In sum, our finding that three distinct agents can increase the potency of **C10** reveals that there are multiple routes by which cancer cells can be sensitized to the cytotoxic effects of WINi, including combining WINi with existing FDA-approved therapeutics.

**Venetoclax Is Synergistic with WINi in a Disseminated Leukemia Model.** We next asked whether synergy between **C10** and venetoclax generally occurs in AML cell lines. We treated OCI-AML-2, OCI-AML-3, and OCI-AML-5, as well as MOLM-13 and MV4:11, cells for 4 d with an 8 × 8 dose matrix of each agent, and calculated the extent of cellular inhibition, where 100% corresponds to complete cell death. Again, synergy data are well fit to the MuSyC equation (*SI Appendix*, Fig. S4*A*), and again there is modest synergy of efficacy with the two agents, the most notable being a 50% increase in the maximal effect with the combination in OCI-AML-5 cells (*SI Appendix*, Fig. S4*B*). Also as before, we observe robust bidirectional synergy of potency in two of the three additional AML lines tested (Fig. 5*A*). The exception here is OCI-AML-3 cells, which are resistant to venetoclax (29). MuSyC isobole analysis revealed that, in combination with venetoclax, the maximal effects of **C10** in these additional sensitive lines are achieved at 100-fold lower doses of **C10** and 25- (OCI-AML-5) or seven-(OCI-AML-2) fold lower doses of venetoclax (Fig. 5*B*) than would be expected in the absence of synergy. This effect is comparable to the dose reductions observed in parallel analysis of MOLM-13 and MV4:11 cells (*SI Appendix*, Fig. S4*C*). Thus, in AML cells that are capable of responding to the drug, we may expect that venetoclax will substantially increase the potency of WINi.

To determine whether the synergy we observe is consistent with the mechanism of action of each agent, we performed RNA-sequencing (RNA-Seq) on MV4:11 cells treated for 72 h with 100 nM **C10,** 50 nM venetoclax, or both (Dataset S3). These concentrations were chosen as the dose pair yielding the highest increase in activity over either single agent. Alone, **C10** and venetoclax produce distinct transcriptomic responses (*SI Appendix*, Fig. S4*D*). Consistent with its mechanism of action, **C10** suppresses expression of genes connected to the cell cycle, the ribosome, and MYC (*SI Appendix*, Fig. S4*E*). And it induces sets of genes connected to the lysosome, p53, apoptosis, and oxidative phosphorylation (*SI Appendix*, Fig. S4*F*). Venetoclax treatment alone leads to suppression of similar types of genes, including those connected to the ribosome (*SI Appendix*, Fig. S4*E*); it also leads to induction of genes connected to oxidative phosphorylation, apoptosis, and p53 (*SI Appendix*, Fig. S4*F*). Most gene expression changes produced with single agents persist in the combination (*SI Appendix*, Fig. S4*D*), but new ones also appear. At genes specifically dysregulated in the **C10**/venetoclax combination, we see suppression of transcripts linked to splicing, translation, and MYC, and induction of transcripts linked to TNFα and Notch signaling, and p53 (Fig. 5*C*). Focusing on the p53 response, we observe that fewer consensus p53 target genes (30) are altered in the combination treatment than with **C10** alone (*SI Appendix*, Fig. S4*G*), and there tends to be a shift in the expression of p53 target genes that favors apoptosis: Proapoptotic p53 target genes such as HES1 (31), PLK2 and PLK3 (32), and NOXA (33) are all more strongly induced by the **C10**/venetoclax combination (Fig. 5*D*), whereas **C10**-mediated induction of CDKN1A (p21)—which effects cell cycle arrest in response to p53 activation (34)—is blocked by addition of venetoclax. This shift is consistent with the ability of venetoclax to modify the p53 response to one that is more profoundly linked to cell death (35), and it is likely a direct effect of the drug: As early as 6 h after treatment, we observe that induction of p21 by **C10** is tempered by the combination with venetoclax, whereas cleaved PARP1 (an indicator of apoptosis) is induced (Fig. 5*E*).

Finally, we asked whether **C10** displays synergy of potency with venetoclax in vivo, using a disseminated MV4:11 transplantation model in NSGS mice (36). After establishing leukemia, mice were dosed orally with 20 mg/kg venetoclax, 100 mg/kg **C10**, or both, for 4 wk, and leukemia burden measured by tracking human chimerism with anti-human CD45 antibodies. Individually, at the doses examined, both agents moderately suppressed the extent of chimerism, most notably in the blood and to a lesser extent in the bone marrow and spleen (Fig. 5 *F* and *G*). In combination, however, tumor burden was lower in all three compartments. Accordingly, spleen weight was also reduced in the combination compared to the individual treatments (*SI Appendix*, Fig. S4*H*). The combination was well tolerated during the treatment period, with mice showing no signs of clinical abnormalities or significant weight loss (*SI Appendix*, Fig. S4*I*). Thus, as predicted from in vitro synergy studies, highly effective anti-leukemia activity can be achieved with combination of WINi with the FDA-approved agent venetoclax in vivo.

## Discussion

Despite excitement over their potential, WINi have suffered a lack of clarity in terms of when and how they can best be deployed for future cancer therapy. Concerns over targeting a panessential protein, a unique mechanism of action, and an absence of systematic screening across cancer cell panels have conspired to keep the potential therapeutic applications of WINi opaque. This study remedies these deficits by screening WINi against a diverse collection of cancer cell lines, alone and in combination with other anticancer agents. Our findings extend the potential utility of WINi beyond the current handful of rare cancer types, highlight

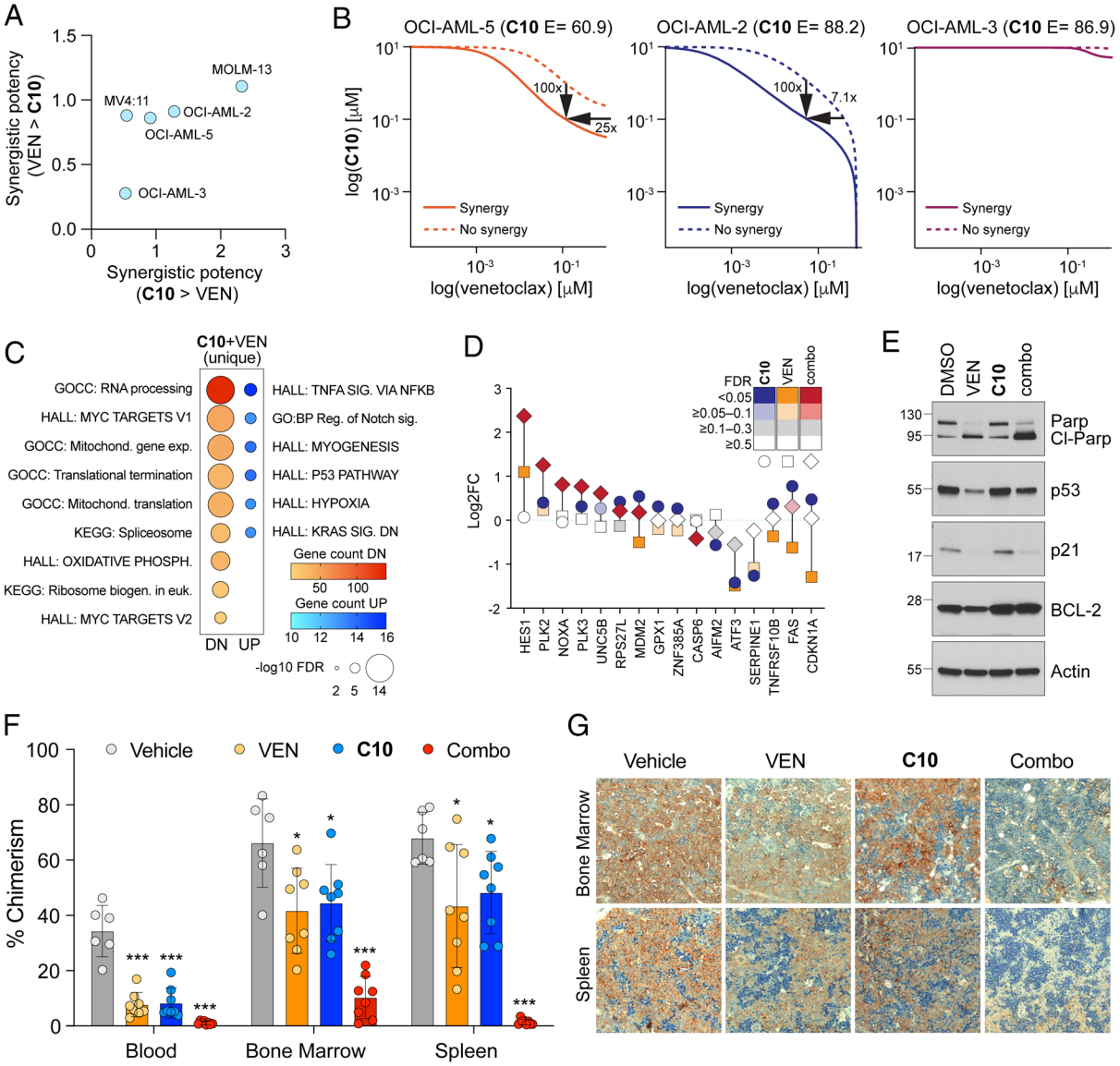


**Fig. 5.** Venetoclax is synergistic with WINi in AML cells in vitro and in vivo. (*A*) Synergistic potency scatterplot for the **C10** and venetoclax combination in each of the cell lines. "**C10** > VEN" denotes the impact of **C10** on the potency of venetoclax. "VEN > **C10**" denotes the impact of venetoclax on the potency of **C10**. ($n = 3$). (*B*) MuSyC isobole analysis of the combination of **C10** and venetoclax in OCI-AML-5, OCI-AML-2, and OCI-AML-3 cells. Dose combinations required to maintain the maximal effect of **C10** alone ("E") are traced by lines, with (solid) or without (dashed) synergy. (*C*) Output of gene enrichment analysis for genes uniquely suppressed (DN) or induced (UP) following 72 h of treatment of MV4:11 cells with 100 nM **C10** and 50 nM venetoclax, as determined by RNA-Seq ($n = 3$). "GOCC" = GO cellular component; "HALL" = Hallmark.MSigDB pathways. Circle size represents −log10 of the FDR; color represents the recovered gene count for each pathway. (*D*) Graph showing the log2 fold-change (Log2FC) in the mRNA levels of select p53 consensus target genes (30), compared to dimethyl sulfoxide (DMSO) controls, in MV4:11 cells treated for 72 h with 100 nM **C10**, 50 nM venetoclax (VEN), or both (combo). (*E*) Western blotting analysis of PARP-1 (Parp), cleaved PARP-1 (Cl-Parp), p53, p21, BCL-2, and actin (loading control) in lysates prepared from MV4:11 cells treated with DMSO, 50 nM venetoclax (VEN), 100 nM **C10**, or both (combo) for 6 h. Representative images from three biological replicates are shown. (*F*) Irradiated NSGS mice were injected with $10^6$ MV4:11 cells via the tail vein and leukemia cells allowed to engraft for 6 d. Mice were treated by oral gavage with vehicle (daily), venetoclax (VEN; 20 mg/kg five days/week), **C10** (100 mg/kg daily), or both (Combo—VEN; 20 mg/kg five days/week/**C10** 100 mg/kg daily) for 28 d. Percent chimerism, a measure of tumor burden, was determined by flow cytometry to quantify the percentage of human CD45-positive cells present in the blood, bone marrow, or spleen at time of killing. Bars represent mean% $CD45^+$ cells, error bars are SD, individual data points for each mouse are shown by colored circles. Statistical significance determined by the *t* test. $*P < 0.05$; $***P < 0.001$. $n = 6$ mice vehicle group, 8 for other groups. (*G*) Immunohistochemistry of leukemia cells in bone marrow (femur) and spleen in representative mice from each of the treatment groups, stained with a monoclonal antibody against human CD45; images taken with 20× magnification.

hematologic malignancies as a particularly sensitive cancer cohort, and demonstrate that WINi can be combined with the FDA-approved drug venetoclax to effectively suppress AML in vivo.

There are a number of important implications of this work, one of which is the demonstration that a common essential protein such as WDR5 (10) can be targeted by site-selective inhibitors to effect specific cancer cell inhibition. Both transcriptomic (9) and proteomic (37) studies have demonstrated that WINi disrupt only a subset of the activities/interactions in which WDR5 is involved, leading us to conclude that WINi are selective loss of function agents. This point is reinforced by the dichotomy we observe between the sensitivity of cancer cells to WIN site inhibition versus WDR5 depletion. We do not understand which of the many functions of WDR5 (2) are essential in most cells, but given the picomolar potency of WINi used in our screening, we can reasonably conclude that it is unrelated to a function that depends on the integrity of the WIN site—including RPG transcription (6). Although the selective action of WINi makes it impossible to use resources such as DepMap (10) to inform potential utility, it is worth

emphasizing that this selectivity may also underlie the safety of these agents in vivo, as **C10** is extremely well-tolerated in rats and mice (5), despite 100% sequence identity between human and rodent WDR5. Further studies are needed to investigate the action of WINi in normal tissues and to understand the molecular basis through which these agents are safe.

Until now, MLLr AML was the only type of hematologic malignancy known to be sensitive to WIN site blockade (1). Our finding of the broad sensitivity of leukemia and lymphoma cells to WINi, both in vitro and in vivo, thus represents a significant expansion in the number of cancer instances that could benefit from WINi in the clinic. Within hematologic cancer lines, we find that sensitivity to WINi correlates with expression of genes connected to protein synthesis—a finding that is consistent with the mechanism of action of these agents (12) and one that could potentially be developed in the future into a rationalized set of patient selection criteria. Notably, DLBCL are among the cancer lines most sensitive to WINi, which is consistent with the prominence of c-MYC in the etiology of these cancers (38). Surprisingly, however, we also find that the response of DLBCL cells to WINi is not obligatorily linked to WT p53 status. Further studies will be required to dissect p53-independent responses to WINi, but this observation is important because it demonstrates that, contrary to current thinking, retention of intact p53 signaling is not an invariant barrier to the action of these agents against cancer cells.

Another important aspect of this work is our finding that some solid cancer cell lines, particularly those derived from ovarian and breast cancers, are sensitive to WINi in vitro. Other than a recent report showing estrogen receptor-positive breast cancer cell stemness depends on WDR5 (39), little if any work has been done to systematically probe the effects of WINi on ovarian and breast cancer cell function to date. Therefore, pursuing WDR5 inhibitors in the context of these cancers is promising and has the potential to uncover therapeutic opportunities for these malignancies with a significant clinical burden.

As combination approaches to treat cancer offer the most promise clinically, we sought to determine the efficacy of WINi when combined with additional anticancer agents, especially those with FDA-approval. In doing so, we observed actionable drug combination strategies that should be front-lined for clinical evaluation, particularly for the treatment of AML. Two therapeutics rising to the top of our synergy assays are doxorubicin and venetoclax, both of which are FDA-approved for the treatment of AML. Supporting this result, we found that WINi are highly effective when combined with venetoclax for inhibition of AML in a disseminated model of the disease, providing compelling data supporting the combination of WINi and venetoclax for the treatment of blood cancers.

Even with advances in using venetoclax for the treatment of myeloid disease, resistance continues to be a significant challenge. Combining venetoclax with other agents in the clinic is demonstrated to help overcome these hurdles (40–42). Furthermore, given the potent bidirectional synergy between **C10** and venetoclax, our data indicate that it may be possible to use drug combinations to mitigate possible toxicities associated with either agent. Although venetoclax is a targeted anticancer agent, myelosuppression is a frequent complication with standard dosing regimens (43). Therefore, mitigating this toxicity with lower dosing by combining with WINi is an attractive future clinical application.

In conclusion, based on our study we propose that—if WINi prove safe and tolerable in humans—clinical vetting of these agents should initially be focused on hematologic malignancies and that combination treatment of WINi with venetoclax be prioritized for evaluation against AML. Moreover, as WT p53 status is no longer a barrier to the effectiveness of WINi, and as solid cancer cell lines can be as sensitive to WINi as those derived from hematologic malignancies, we propose that additional single agent and combination screening be conducted to further expand the malignant settings in which WINi can be employed for cancer therapy.

## Materials and Methods

**Compound Synthesis and Characterization.** Detailed methods for the synthesis and characterization of compounds **C3b** and **C38b** are described in *SI Appendix, Materials and Methods*. Protocols for the synthesis of **C40** (44) and **C10** (5) have been described.

**Cell lines, Screening, and Analysis.** Detailed information on cell lines, culture conditions, single agent and combination (synergy) profiling, and subsequent analysis methods are described in *SI Appendix, Materials and Methods*. Single agent screening of **C3b**, **C38b**, and **C40** in the OncoSignature 2D Cell Panel, and synergy screening of **C10** in leukemia and lymphoma lines, were performed by Horizon Discovery.

**Molecular Biology.** Methods for western blotting, RNA-Seq, and RNA-Seq bioinformatics analysis are described in *SI Appendix, Materials and Methods*.

**Subcutaneous Mouse Xenograft Assays.** Experimental methods for analysis of the sensitivity of hematological cancer cell lines to **C10** in subcutaneous mouse xenograft assays are described in *SI Appendix, Materials and Methods*. These experiments were conducted by Pharmaron, Inc. All animal studies were reviewed and approved by the Institutional Animal Care and Use Committee of Pharmaron.

**Disseminated Leukemia Model.** Detailed methods for analysis of the sensitivity of MV4:11 cells to **C10** and venetoclax (alone and in combination) are provided in *SI Appendix, Materials and Methods*. All animal experiments were conducted in accordance with guidelines approved by the Institutional Animal Care and Use Committee at Vanderbilt University Medical Center. Flow cytometry (to follow chimerism) and immunohistochemistry methods are also described in *SI Appendix, Materials and Methods*.

**MuSyC Analysis.** Synergy data were fit to the 2D Hill equation following the procedure described in ref. 25. Full details, including a description of the newly developed MuSyC isobole analysis, are described in *SI Appendix, Materials and Methods*.

**Quantification and Statistical Analysis.** The *n* for each experiment, representing biological replicates, can be found in the figure legends. The statistical test and threshold for statistical significance for each experiment is also provided.

**Data, Materials, and Software Availability.** Genomic data generated in this study are publicly available in Gene Expression Omnibus (GEO) at GSE136451 (45). All other data are included in the article and/or supporting information.

**ACKNOWLEDGMENTS.** The VANTAGE Shared Resource is supported by the Clinical and Translational Science Awards Grant (RR024975), the Vanderbilt Ingram Cancer Center (CA068485), the Vanderbilt Vision Center (EY008126), the Vanderbilt Translational Pathology Shared Resource (CA068485), and NIH/National Center for Research Resources (RR030956). We thank Vanderbilt University High-Throughput Screening (CA068485), Biomolecular NMR (NIH SIG Grant 1S-10RR025677), and Mass Spectrometry Research Centers (CA068485). We thank other contributing and supporting members of the Division of Cancer Treatment and Diagnosis at the National Cancer Institute (NCI), the NCI Chemical Biology Consortium, Horizon Discovery Ltd., and Pharmaron, Inc. for their contributions. B.N.S. was supported by a grant from the NIH/NCI (CA090625). B.C.G. was supported by grants from the NIH/NCI (CA090625, F32CA268703, T32CA217834) and the Conquer Cancer Foundation. C.T.M. was supported by a K99 from the NIH/National Institute of Allergy and Infectious Diseases (AI175656). M.R.S. receives funding from the Adventure Alle Fund, Beverly and George Rawlings Endowment, Biff Ruttenberg Foundation, and the NIH (CA262287 and OH012271). A.J.S. was supported by a grant from the NIH/National Instituteof Diabetes and Digestive and Kidney Diseases (DK127699).

This work was supported by awards from the NIH/NCI–under Chemical Biology Consortium Contract No. HHSN261200800001E (S.W.F., and W.P.T.), P50 CA236733 (S.W.F., and W.P.T.), and CA200709 (W.P.T.)–as well as grants from the Robert J. Kleberg, Jr., and Helen C. Kleberg Foundation (S.W.F., and W.P.T.). M.R.S. receives research funding from ALX Oncology, Astex, Incyte, Takeda and TG Therapeutics.

Author affiliations: [a]Department of Molecular, Cellular, and Developmental Biology, University of Colorado Boulder, Boulder, CO 80309; [b]Duet BioSystems, Nashville, TN 37212; [c]Department of Pediatrics, Vanderbilt University Medical Center, Nashville, TN 37232; [d]Department of Biostatistics, Vanderbilt University Medical Center, Nashville, TN 37232; [e]Center for Quantitative Sciences, Vanderbilt University Medical Center, Nashville, TN 37232; [f]Department of Biochemistry, Vanderbilt University School of Medicine, Nashville, TN 37240; [g]Department of Medicine, Vanderbilt University Medical Center, Nashville, TN 37232; [h]Department of Cell and Developmental Biology, Vanderbilt University School of Medicine, Nashville, TN 37240; [i]Leidos Biomedical Research, Frederick National Laboratory for Cancer Research, Frederick, MD 21701-4907; [j]Chemical Biology Laboratory, Center for Cancer Research, National Cancer Institute, Frederick, MD 21702-1201; [k]Department of Biology, Middle Tennessee State University, Murfreesboro, TN 37132; [l]Department of Pharmacology, Vanderbilt University School of Medicine, Nashville, TN 37240; and [m]Department of Chemistry, Vanderbilt University, Nashville, TN 37240

Author contributions: B.N.S., B.C.G., G.C.H., G.M.S., W.J.M., T.L., M.R.S., A.M.W., V.Q., S.W.F., and W.P.T. designed research; C.T.M., B.N.S., J.W., K.B.T., B.C.G., A.J.S., and S.L.L. performed research; C.T.M. and K.B.T. contributed new reagents/analytic tools; C.T.M., B.N.S., J.W., K.B.T., G.C.H., A.J.S., G.M.S., T.L., M.R.S., A.M.W., Q.L., and W.P.T. analyzed data; C.T.M., M.R.S., S.W.F., and W.P.T. acquired funding; and C.T.M., B.N.S., J.W., K.B.T., B.C.G., G.C.H., G.M.S., W.J.M., T.L., M.R.S., A.M.W., Q.L., V.Q., S.W.F., and W.P.T. wrote the paper.

Competing interest statement: Fesik, S. W., Stauffer, S. R., Salovich, J. M., Tansey, W. P., Wang, F., Phan, J., Olejniczak, E. T., inventors. WDR5 inhibitors and modulators. United States Patent US 10,501,466. 10 December 2019. Fesik, S. W., Stauffer, S. R., Tansey, W. P., Olejniczak, E. T., Phan, J., Wang, F., Jeon, K., Gogliotti, R. D., inventors. WDR5 inhibitors and modulators. United States Patent US 10,160,763. 25 December 2018. Lee. T.; Alvarado, J.; Tian, J.; Meyers, K. M.; Han, C.; Mills, J. J.; Teuscher, K. B.; Fesik, S. W. WDR5 inhibitors and modulators. WO 2020086857. 30 April 2020. Lee. T.; Han, C.; Mills, J. J.; Teuscher, K. B.; Tian, J.; Meyers, K. M.; Chowdhury, S.; Fesik, S. W. WDR5 inhibitors and modulators. WO 2020247679. 10 December 2020. Lee. T.; Teuscher, K. B.; Tian, J.; Meyers, K. M.; Chowdhury, S.; Fesik, S. W. WDR5 Inhibitors and modulators. WO 2021092525. 14 May 2021. Lee. T.; Teuscher, K. B.; Chowdhury, S.; Tian, J.; Meyers, K. M.; Fesik, S. W. WDR5 Inhibitors and modulators. WO2022236101. 10 November 2022. C.T.M. and V.Q. are co-founders of Duet BioSystems. M.R.S. has stock in Karyopharm and Ryvu; serves on advisory boards or consults for BMS, CTI, Forma, Geron, GSK, Karyopharm, Rigel, Ryvu, Taiho and Treadwell. All other authors declare no competing interest.

1. A. M. Weissmiller, S. W. Fesik, W. P. Tansey, WD repeat domain 5 inhibitors for cancer therapy: Not what you think. *J. Clin. Med.* **13**, 274 (2024), 10.3390/jcm13010274.
2. A. D. Guarnaccia, W. P. Tansey, Moonlighting with WDR5: A cellular multitasker. *J. Clin. Med.* **7**, 21 (2018), 10.3390/jcm7020021.
3. E. R. Aho *et al.*, Displacement of WDR5 from chromatin by a WIN site inhibitor with picomolar affinity. *Cell Rep.* **26**, 2916–2928.e13 (2019).
4. E. T. B. Antunes, K. Ottersbach, The MLL/SET family and haematopoiesis. *Biochim. Biophys. Acta Gene Regul. Mech.* **1863**, 194579 (2020), 10.1016/j.bbagrm.2020.194579.
5. K. B. Teuscher *et al.*, Structure-based discovery of potent WD repeat domain 5 inhibitors that demonstrate efficacy and safety in preclinical animal models. *Proc. Natl. Acad. Sci. U.S.A.* **120**, e2211297120 (2023), 10.1073/pnas.2211297120.
6. A. F. Bryan *et al.*, WDR5 is a conserved regulator of protein synthesis gene expression. *Nucleic Acids Res.* **48**, 2924–2941 (2020).
7. A. C. Florian *et al.*, Synergistic action of WDR5 and HDM2 inhibitors in SMARCB1-deficient cancer cells. *NAR Cancer* **4**, zcac007 (2022), 10.1093/narcan/zcac007.
8. F. Cao *et al.*, Targeting MLL1 H3K4 methyltransferase activity in mixed-lineage leukemia. *Mol. Cell* **53**, 247–261 (2014).
9. A. J. Siladi *et al.*, WIN site inhibition disrupts a subset of WDR5 function. *Sci. Rep.* **12**, 1848 (2022), 10.1038/s41598-022-05947-9.
10. A. Tsherniak *et al.*, Defining a cancer dependency map. *Cell* **170**, 564–576.e16 (2017).
11. L. R. Thomas *et al.*, Interaction of the oncoprotein transcription factor MYC with its chromatin cofactor WDR5 is essential for tumor maintenance. *Proc. Natl. Acad. Sci. U.S.A.* **116**, 25260–25268 (2019).
12. G. C. Howard *et al.*, Ribosome subunit attrition and activation of the p53-MDM4 axis dominate the response of MLL-rearranged cancer cells to WDR5 WIN site inhibition. *Elife* **12**, RP90683 (2024), 10.7554/eLife.90683.
13. J. Pelletier, G. Thomas, S. Volarevic, Ribosome biogenesis in cancer: New players and therapeutic avenues. *Nat. Rev. Cancer* **18**, 51–63 (2018).
14. J. Tian *et al.*, Discovery and structure-based optimization of potent and selective WD repeat domain 5 (WDR5) inhibitors containing a dihydroisoquinolinone bicyclic core. *J. Med. Chem.* **63**, 656–675 (2020).
15. J. M. Dempster *et al.*, Chronos: A cell population dynamics model of CRISPR experiments that improves inference of gene fitness effects. *Genome Biol.* **22**, 343 (2021), 10.1186/s13059-021-02540-7.
16. W. Li *et al.*, Targeting MYC activity in double-hit lymphoma with MYC and BCL2 and/or BCL6 rearrangements with epigenetic bromodomain inhibitors. *J. Hematol. Oncol.* **12**, 73 (2019), 10.1186/s13045-019-0761-2.
17. M. Ghandi *et al.*, Next-generation characterization of the Cancer Cell Line Encyclopedia. *Nature* **569**, 503–508 (2019).
18. M. Molica, C. Mazzone, P. Niscola, P. de Fabritiis, TP53 mutations in acute myeloid leukemia: Still a daunting challenge? *Front. Oncol.* **10**, 610820 (2020), 10.3389/fonc.2020.610820.
19. F. N. van Leeuwen, Therapeutic targeting of mutated p53 in acute lymphoblastic leukemia. *Haematologica* **105**, 10–11 (2020).
20. J. Barretina *et al.*, The Cancer Cell Line Encyclopedia enables predictive modelling of anticancer drug sensitivity. *Nature* **483**, 603–607 (2012).
21. J. Camps *et al.*, Genomic imbalances and patterns of karyotypic variability in mantle-cell lymphoma cell lines. *Leuk. Res.* **30**, 923–934 (2006).
22. R. J. Jones *et al.*, Inhibition of the p53 E3 ligase HDM-2 induces apoptosis and DNA damage-independent p53 phosphorylation in mantle cell lymphoma. *Clin. Cancer Res.* **14**, 5416–5425 (2008).
23. R. Bayat Mokhtari *et al.*, Combination therapy in combating cancer. *Oncotarget* **8**, 38022–38043 (2017).
24. C. T. Meyer *et al.*, Quantifying drug combination synergy along potency and efficacy axes. *Cell Syst.* **8**, 97–108.e16 (2019).
25. D. J. Wooten, C. T. Meyer, A. L. R. Lubbock, V. Quaranta, C. F. Lopez, MuSyC is a consensus framework that unifies multi-drug synergy metrics for combinatorial drug discovery. *Nat. Commun.* **12**, 4607 (2021), 10.1038/s41467-021-24789-z.
26. D. H. Lee, C. Kim, L. Zhang, Y. J. Lee, Role of p53, PUMA, and Bax in wogonin-induced apoptosis in human cancer cells. *Biochem. Pharmacol.* **75**, 2020–2033 (2008).
27. A. L. Latif *et al.*, BRD4-mediated repression of p53 is a target for combination therapy in AML. *Nat. Commun.* **12**, 241 (2021), 10.1038/s41467-020-20378-8.
28. A. J. Souers *et al.*, ABT-199, a potent and selective BCL-2 inhibitor, achieves antitumor activity while sparing platelets. *Nat. Med.* **19**, 202–208 (2013).
29. J. Bogenberger *et al.*, Combined venetoclax and alvocidib in acute myeloid leukemia. *Oncotarget* **8**, 107206–107222 (2017).
30. M. Fischer, Census and evaluation of p53 target genes. *Oncogene* **36**, 3943–3956 (2017).
31. T. Kato *et al.*, Hes1 suppresses acute myeloid leukemia development through FLT3 repression. *Leukemia* **29**, 576–585 (2015).
32. J. P. Bewersdorf, A. M. Zeidan, Polo-like kinase inhibition as a therapeutic target in acute myeloid leukemia. *Oncotarget* **12**, 1314–1317 (2021).
33. E. Oda *et al.*, Noxa, a BH3-only member of the Bcl-2 family and candidate mediator of p53-induced apoptosis. *Science* **288**, 1053–1058 (2000).
34. W. S. el-Diry *et al.*, WAF1/CIP1 is induced in p53-mediated G1 arrest and apoptosis. *Cancer Res.* **54**, 1169–1174 (1994).
35. R. Pan *et al.*, Synthetic lethality of combined Bcl-2 inhibition and p53 activation in AML: Mechanisms and superior antileukemic efficacy. *Cancer Cell* **32**, 748–760.e6 (2017).
36. H. E. Ramsey *et al.*, BET inhibition enhances the antileukemic activity of low-dose venetoclax in acute myeloid leukemia. *Clin. Cancer Res.* **27**, 598–607 (2021).
37. A. D. Guarnaccia *et al.*, Impact of WIN site inhibitor on the WDR5 interactome. *Cell Rep.* **34**, 108636 (2021), 10.1016/j.celrep.2020.108636.
38. S. Martinez-Martin, M. E. Beaulieu, L. Soucek, Targeting MYC-driven lymphoma: Lessons learned and future directions. *Cancer Drug Resist.* **6**, 205–222 (2023).
39. C. P. Pai *et al.*, The PML1-WDR5 axis regulates H3K4me3 marks and promotes stemness of estrogen receptor-positive breast cancer. *Cell Death Differ.* **31**, 768–778 (2024), 10.1038/s41418-024-01294-6.
40. M. R. Savona, J. C. Rathmell, Mitochondrial homeostasis in AML and gasping for response in resistance to BCL2 blockade. *Cancer Discov.* **9**, 831–833 (2019).
41. C. D. DiNardo *et al.*, Azacitidine and venetoclax in previously untreated acute myeloid leukemia. *N. Engl. J. Med.* **383**, 617–629 (2020).
42. S. Pei *et al.*, Monocytic subclones confer resistance to venetoclax-based therapy in patients with acute myeloid leukemia. *Cancer Discov.* **10**, 536–551 (2020).
43. G. Richard-Carpentier *et al.*, Clinical experience with venetoclax combined with chemotherapy for relapsed or refractory T-cell acute lymphoblastic leukemia. *Clin. Lymphoma Myeloma Leuk.* **20**, 212–218 (2020).
44. K. B. Teuscher *et al.*, Discovery of potent orally bioavailable WD repeat domain 5 (WDR5) inhibitors using a pharmacophore-based optimization. *J. Med. Chem.* **65**, 6287–6312 (2022).
45. W. P. Tansey, A. Foshage, A. Weissmiller, Q. Liu, WDR5 is a conserved regulator of protein synthesis gene expression. Gene Expression Omnibus. https://www.ncbi.nlm.nih.gov/geo/query/acc.cgi?acc=GSE136451. Deposited 27 August 2019.